ROYAL SOCIETY
OF CHEMISTRY

EDGE ARTICLE

Check for updates

On/off porosity switching and post-assembly modifications of Cu_4L_4 metal–organic polyhedra†

Witold M. Bloch, [ID] *[a] Ravichandar Babarao [ID] [bc] and Matthew L. Schneider [ID] [a]

Synthetic porous materials composed of metal–organic polyhedra (MOPs) have found application in topical areas such as gas storage, separation and catalysis. Control over their physical properties (*e.g.* porosity) has typically been achieved through ligand design or judicious choice of metal ions. Here, we demonstrate pore-size control and on/off porosity in Cu_4L_4 MOPs by exploiting their structural non-rigidity. We report an aldehyde-functionalised MOP (**1**) that can be isolated in five distinct solvatomorphs, each exhibiting different structural flexibility. When soaked in MeOH, two of these solvatomorphs undergo a rapid transformation to a thermodynamically favoured phase, whilst in acetone they template the crystallisation of an entirely new crystal packing. We support these findings by single and powder X-ray diffraction and rationalise the observed phase transformations by lattice energy calculations. Of the five solvatomorphs, three can be obtained as solvent-exchanged pseudo-polymorphs with distinct porosities in their activated form (SA_{BET} = 35–455 m^2 g^{-1}). Further control over the crystal packing of MOPs is achieved through covalent post-assembly modifications, which promote the crystallisation of isoreticular 2-D sheet-like structures.

Introduction

Molecular solids based on cage compounds have recently emerged as an attractive class of porous materials owing to their solution processability and intrinsic porosity.[1–3] Unlike metal–organic frameworks (MOFs)[4] and covalent–organic frameworks (COFs),[5] discrete cage compounds crystallise by virtue of weak intermolecular interactions and thus tend to exhibit a rich crystal-packing behaviour. This is particularly true for purely organic cages, which have been reported to exhibit impressive properties such modular co-crystallisations,[6] guest-induced breathing[7] and on/off porosity switching.[8–10] The crystal-packing behaviour of cage materials formed *via* metal–ligand bonding, however, has not been examined to the same extent, despite the exciting opportunities that these solids offer for gas adsorption[11–13] and catalysis.[14]

Metal–organic polyhedra (MOPs) are a class of discrete nanocages commonly formed by the self-assembly of dicarboxylate linkers and bimetallic paddle-wheels nodes (*e.g.* Cu_2, Rh_2 and Cr_2).[2,12,15] Solvent molecules typically occupy the apical coordination sites of the paddle-wheel nodes, and thus, desolvation allows access to unsaturated metal centres. This

feature has motivated extensive studies examining MOPs for selective gas adsorption[16] and heterogeneous catalysis.[14,17,18] However, the crystal engineering of MOP solids is an area dominated more by serendipity than design; the weak intermolecular interactions that direct the crystal packing of MOPs can depend on the nature of the paddlewheel-bound solvent, making it possible to crystallise different solvatomorphs of the same cage compound.[19] To add to the complexity, solvent exchange processes employed en-route to activation can lead to unknown crystalline or amorphous phases,[12] making it difficult to control the pore-size and porosity of MOPs. Therefore, gaining control over the crystal packing of MOPs, and hence their physicochemical properties, remains a challenge.

Much of the efforts aiming to design MOP-based solids have focused on immobilising MOP particles in mesoporous supports,[20,21] or on approaches that increase intermolecular interactions in the solid-state. For example, introducing ligand-based functionalities such as alkyl substituents,[22] bulky hydrophobic groups,[23] or coordinative O-donors[24] has led to more robust and structurally rigid crystal packings. Owing to the solubility of MOPs, covalent post-assembly modifications (PAM)[25] have also been carried out to modify the interior[26] or exterior surface functionality.[27] However, the development of covalent PAM on paddlewheel-based MOPs is still an emerging field of study, with only a few examples reported.

Herein we show that the crystal-packing and porosity of MOPs can be controlled in the same way as their purely organic analogues; by taking advantage of their rich phase behaviour and amenability to PAM. Thus, we report the synthesis and

[a]Department of Chemistry, The University of Adelaide, Adelaide, Australia. E-mail: witold.bloch@adelaide.edu.au; Tel: +61 8 8313 5039
[b]School of Science, RMIT University, Melbourne, Victoria 3001, Australia
[c]CSIRO, Normanby Road, Clayton 3168, Victoria, Australia

characterisation of an aldehyde-functionalised Cu_4L_4 MOP (**1**, Fig. 1a). By varying the crystallisation conditions, **1** can be obtained in five distinct solvatomorphs with different structural flexibilities. This is demonstrated by phase-dependant transformations which we characterise by X-ray diffraction and rationalise by lattice energy calculations. We show that the activation and porosity of **1** is phase dependant, and non-porous forms can be switched to porous forms by solvent treatment (Fig. 1b). Owing to the solubility of **1**, PAM carried out at the cage exterior facilitate control over the crystal packing by favouring the formation of 2-D sheet-like motifs (Fig. 1c).

Results and discussion

Synthesis and structure of 1a

LH_2 (Fig. 2a) was synthesised in two steps, starting with a Sonogashira cross-coupling of 3,5-dibromobenzaldehyde and methyl 3-ethynylbenzoate. The methyl ester compound was then hydrolysed under mild conditions to afford LH_2 in an overall yield of 64% (ESI†).

Self-assembly of LH_2 with 1.1 equivalents of $Cu(OAc)_2 \cdot 2H_2O$ in DMF resulted in the formation of a soluble Cu_4L_4 lantern cage (**1**) as indicated by ^{1}H NMR spectroscopy and UV-Vis spectroscopy (Fig. S6†).[26,28] Owing to the anomalous magnetic moment of the Cu_2 paddlewheel,[29] proton resonances not immediately adjacent to the metal nodes could be resolved in the ^{1}H NMR spectrum of **1**.‡ For example, the aldehyde resonance of **1** appears upfield shifted relative to the free ligand (*ca.* −0.2 ppm, Fig. 2c). Slow-vapour diffusion of MeOH into a DMF solution of **1** over a period of 5 days yielded rhombohedral crystals of **1a** in 87% yield (based on CHN analysis). Single-crystal X-ray analysis (SCXRD) revealed that **1a** crystallises in the triclinic space group $P\bar{1}$ with half of two crystallographically independent cages in the asymmetric unit. Closer inspection revealed that the ligand backbones in one cage molecule adopt a flattened conformation when viewing the cage down the axis of the Cu_2 paddlewheels. These nodes are coordinated by four carboxylate ligands and two axial DMF ligands. The second
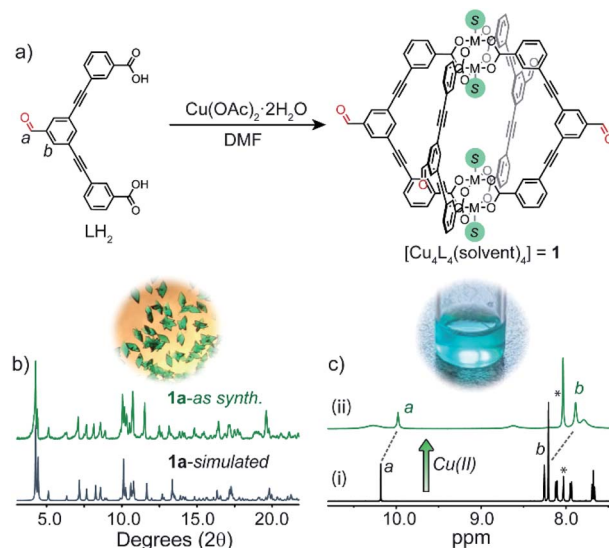

Fig. 2 (a) A scheme showing the self-assembly of **1** in solution from LH_2 and $Cu(OAc)_2$ (S = solvent); (b) simulated and experimental PXRD patterns of phase **1a**; (c) ^{1}H NMR spectrum (500 MHz/DMF-d_7, 25 °C): (i) LH_2, (ii) LH_2 + $Cu(OAc)_2$ (* indicates solvent peak).‡ Above (b) and (c) are photos of crystals of **1a** (left) and a DMF solution of **1** (right).

crystallographically unique cage adopts a pseudo D_{4h}-symmetric conformation where the ligand backbones arrange in a mutually perpendicular fashion.[19] Here, DMF and H_2O ligands coordinate to the exterior and interior sites of the paddlewheels, respectively. The two chemically unique cage molecules present in the crystal packing of **1a** give an overall formula of $[Cu_4L_4(DMF)_4] \cdot [Cu_4L_4(DMF)_2(H_2O)_2]$ (Fig. 3a and S33†). The extended packing of **1a** is stabilised by multiple intermolecular π–π interactions that exist between the benzaldehyde cores of **1** (closest contact = 3.33 Å). This motif produces ordered channels along the *a* axis (Fig. 3a) with aperture dimensions measuring 3.8 × 6.1 Å (when omitting coordinating solvents).

X-ray structures of solvatomorphs 1b–d

We found that **1** could be reproducibly crystallised in three other distinct solvatomorphs by varying the solvent and precipitant of the slow-vapour diffusion (SVD) crystallisation (Table S1†). The crystals of each phase were suitable for SCXRD analysis and powder X-ray diffraction (PXRD) confirmed that the single crystals were representative of their bulk phases (Fig. 2b and S11–S16†).

Needle-shaped crystals of **1b** were obtained when a mixture of LH_2 and $Cu(OAc)_2 \cdot 2H_2O$ was heated in DMSO at 85 °C for 16 h. The same crystal packing could also be obtained by SVD of MeOH into a DMA solution of **1** (**1b-DMA**, Fig. S13c†), although only the former conditions produced crystals suitable for SCXRD. **1b-DMSO** crystallises in the monoclinic space group $C2/c$ with half of the lantern cage in the asymmetric unit. Both interior and exterior paddlewheel sites are occupied by disordered DMSO ligands to give an overall formula of $[Cu_4L_4(DMSO)_4]$. The crystal packing of **1b** is stabilised by multiple

Fig. 1 A summary of the work presented herein: (a) the lantern structure of MOP **1** (S = solvent); (b) phase cycling and porosity switching by solvent treatment and recrystallisation; (c) post-assembly modifications (PAM) of **1** with control over the crystal-packing.
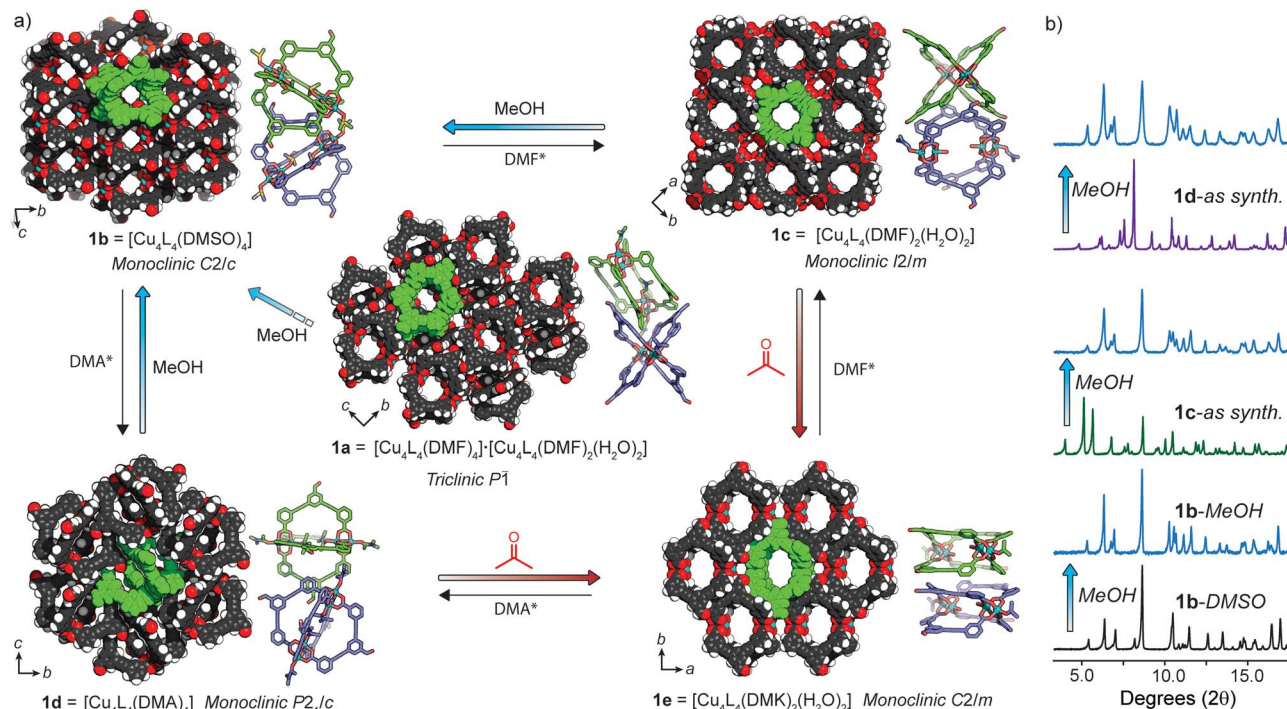
Fig. 3 (a) Single crystal X-ray structures of solvatomorphs **1a–e** in a scheme portraying their structural transformations. The crystal packing of **1a–e** is represented as space-filling (coordinating solvents removed for clarity) and alongside are depictions of the orientations of cage molecules within each phase. Each phase can be regenerated through recrystallisation (*co-solvent = H_2O); (b) PXRD patterns highlighting the solid-state transformations of **1c** and **1d** → **1b** upon exposure to MeOH. Full details of the transformations shown in (a) can be found in the ESI (Fig. S11–S16†).

intermolecular π–π interactions between the phenyl carboxylate and benzaldehyde moieties of **1** (shortest distance = 3.32 Å). This bilateral π-stacking motif results in molecules of **1** arranging in an edge-to-edge fashion. When viewing the extended structure along hkl = 111 plane, open channels intrinsic to the cage structure are evident and measure approximately 4.4 × 4.6 Å in diameter (Fig. 3a).

Slow diffusion of atmospheric moisture into a DMF solution of **1** resulted in the overnight formation of large block-shaped crystals of a new phase (**1c**), as indicated by SCXRD and PXRD analysis. We postulate that under these conditions, **1c** forms in favour of **1a** due to the rapid rate of crystallisation (24 h) compared to DMF/MeOH (5 days).[9] **1c** crystallises in the monoclinic space group $I2/m$, with a quarter of two crystallographically independent cages in the asymmetric unit. In contrast to **1a**, both cage molecules have identical paddlewheel compositions; DMF and H_2O ligands occupy the exterior and interior apical sites, respectively. The overall formula of **1c** is therefore $[Cu_4L_4(DMF)_2(H_2O)_2]$ (Fig. 3a and S33†). Interestingly, the extended structure of **1c** comprises of a mutually perpendicular face-to-face cage packing. This arrangement creates open channels along the a and c axis, with the largest pore dimensions measuring 5.4 × 6.0 Å. However, this packing motif lacks defined π–π interactions and is stabilised by weak hydrogen bonding between the coordinated DMF ligands and the aldehyde group of **1** (C–H···O = 2.31 Å, 119°).

Another distinct crystalline phase could be obtained by slow diffusion of atmospheric moisture into a DMA solution of **1**. **1d** crystallises in the monoclinic space group $P2_1/c$, with half of the lantern cage in the asymmetric unit. In this solvatomorph, both apical coordination sites of the Cu$_2$ paddlewheel are occupied by DMA ligands (Fig. S33†). In the crystal packing of **1d**, cage molecules arrange in an edge-to-edge fashion and exhibit intermolecular π–π interactions between the benzaldehyde and phenyl carboxylate moieties. Despite possessing a similar crystal density to that of **1b** (Table S2†) the arrangement of cage molecules in **1d** does not result in defined solvent-accessible channels (Fig. 3a).

Owing to the solubility of **1** in DMF and DMA, crystals of each phase could be recrystallised to recycle between **1a–d** (Fig. 3a).

Phase transformations of 1

Understanding transformations in porous materials is crucial in relating structure to function. For flexible MOFs, solid-state transformations often involve preservation of metal–ligand connectivity and framework topology, making their characterisation straightforward by PXRD methods.[30,31] In contrast, phase transformations in MOP solids are difficult to elucidate since the weak intermolecular interactions that govern their crystal packing allow for dramatic reorientations of the cage molecules without preservation of single crystallinity. As a result, assigning the structure of solvent exchanged MOP solids is often omitted.

The crystallisation of **1a–d** indicated to us that the solvent and precipitant both contribute in determining the extended packing of the MOP structure. As such, we posited that in the four structures of **1**, the apical paddlewheel solvent stabilises the crystal packing to different degrees. In order to examine this hypothesis, we subjected solvatomorphs **1a–d** to solvent exchange with MeOH and acetone, as these solvents are commonly used en-route to activation.[32,33] With the X-ray structures of **1a–d** in hand, we were able to use powder diffraction to map out the solvent-induced transformations in bulk samples of **1** (Fig. 3b and S11–S16†).

PXRD analysis revealed that both **1a** and **1b** retain their overall crystal packing after solvent exchange with MeOH (Fig. 3b, S11 and S13†). Whilst the methanol exchanged form of **1b** was stable indefinitely, a time-dependant PXRD experiment of **1a** revealed that after 9 h, a slow transformation to **1b** begins to occur and is complete within ∼24 h (Fig. 3a and S12†). In contrast, washing **1c** and **1d** in MeOH resulted in a rapid (<5 minutes) and quantitative transformation to **1b** as indicated by PXRD (Fig. 3b, S14 and S15†). Notably, these conversions proceed entirely in the solid-state as **1** is insoluble in MeOH and DMF/MeOH mixtures (Fig. S8†).§ Although the mechanism of these types of transformations is difficult to elucidate,[8] we speculate that the relative cage re-orientations that occur during this process are different for each phase (Fig. S34†).

Interestingly, we observed a different transformation when solvatomorphs of **1** were immersed in acetone. Whilst **1a** and **1b** retained their crystal packing even after 3 months (Fig. S11 and S13†), **1c** and **1d** both transformed to a new phase (**1e**) over a period of 3 weeks (Fig. S14 and S15†). The crystals of the former sample were of sufficient quality for structural determination by synchrotron SCXRD. **1e** crystallises in the monoclinic space group $C2/m$ and contains a quarter of the cage in the asymmetric unit. Here, the apical sites of the Cu_2 paddlewheel nodes are occupied by exterior acetone (DMK) and interior water ligands to give the formula $[Cu_4L_4(DMK)_2(H_2O)_2]$. The lantern cage adopts an extremely flattened conformation that facilitates close intermolecular π-stacking between the benzaldehyde and phenyl carboxylate moieties (shortest distance = 3.29 Å). The eclipsed face-to-face cage packing results in open channels along the c axis with apertures of 6.0×8.9 Å (Fig. 3a). Unsurprisingly, we found that the PXRD pattern of **1e** remains unchanged upon solvent exchange with MeOH (Fig. S16†).

To further investigate the formation of **1e**, we soaked the as-synthesised crystals of **1c** and **1d** in acetone-d$_6$. Indeed, we observed trace quantities of **1** in the ^{1}H NMR spectrum of the suspension, albeit only in the presence of DMA or DMF; washing the samples further with acetone-d$_6$ (in order to exchange out the remaining solvent) led to the disappearance of resonances originating from **1** (Fig. S8†). As the crystals of **1c** and **1d** do not completely dissolve during the transformation, we suggest that the conversion to **1e** is solvent assisted,[34,35] although a traditional recrystallisation cannot be ruled out. It is noteworthy that **1e** could not be obtained through conventional crystallisation methods or by the conversion of other solvatomorphs (Fig. S17, Table S1†), suggesting that **1c** and **1d** act as crystalline templates for this transformation.

To rationalise the observed transformations we performed lattice energy calculations on the set of five structures based on periodic density functional theory (DFT) calculations as implemented in the software package VASP 5.4.4.[36] We note that lattice energy comparisons are commonly made for purely organic polymorphs (where solvent does not play a structural role).[37,38] Nevertheless, we expected that the relative lattice energies of the desolvated forms of **1a–e** should give insight into their transformations despite their experimental accessibility. In our DFT calculations, electron exchange and correlation were described using the generalised gradient approximation Perdew, Burke, and Ernzerhof (PBE) form[39] and the projector-augmented wave potentials were used to treat core and valence electrons.[40] To account for the long-range dispersion interactions, we included the dispersion corrections using DFT-D3 method.[41] A full optimisation of the structures was performed allowing both the atomic and cell parameters to relax in the absence of the apical paddlewheel solvents. We observed no substantial change in the structural conformation and the lattice parameters for each of the five structures in the DFT optimisation (full details are given in the ESI†). The results of the DFT calculations were consistent with the expected correlation of higher density structures (e.g. **1a**, **1b** and **1e**) being lower in energy compared to structures with lower density (e.g. **1c** and **1d**, Table S6†).[37] As observed experimentally, **1b** is indeed the lowest energy structure within the set of five phases (Table S4†), closely followed by **1e** (+15.3 kJ mol^{-1}, Fig. 4). The fact that these two phases are energetically similar yet do not interconvert through solvent exchange suggests that their crystal packing is stabilised predominantly by intermolecular cage interactions rather than the apical paddlewheel solvent. Relative to **1b**, the lattice energy of **1a** differs by only +22.3 kJ mol^{-1} which is in agreement with its metastability and slow transformation to **1b** in MeOH. On the other hand, the lattices energies of **1c** and **1d** are comparatively higher (+106 kJ mol^{-1} and +69 kJ mol^{-1}, respectively) which also

Fig. 4 Energy landscape of the experimentally observed phases of **1a–e**, relative to **1b**. The calculated lattice energies are based on DFT optimisation including dispersion interactions with apical paddlewheel solvents omitted.

Fig. 6 (a) Scheme illustrating the covalent PAM of **1** to give **2** or **3**; (b) ^{1}H NMR (500 MHz/DMF-d$_7$) of (ii) the reaction mixture of **2** after heating and (i) before heating.‡ Excess aniline shown in grey, *DMF solvent peak; (c) X-ray structure of **2**; (d) perspective view of the crystal packing of **2**; (e) perspective view of the crystal packing of **3**.

interactions and results in an overall 2D sheet-like packing (Fig. 6d). Within this motif, the average Cu···Cu distance between cage units measures 18.7 Å, which is an increase of 3.7 Å compared to the furthest Cu···Cu distance observed in the crystal packing of **1** (**1c** = 15.0 Å).

We also performed covalent PAM of **1** with 9-ethyl-9*H*-carbazol-3-amine due to its solubility and extended aromatic structure. This allowed us to thus further examine extensions to the cage architecture and their subsequent effect on the crystal packing. Once again, ^{1}H NMR spectroscopy revealed a >98% conversion of **1** to **3** under the similar reaction conditions to that of **2** (Fig. S9a†). Slow vapour diffusion of diethyl ether into the reaction mixture yielded X-ray quality crystals of a monoclinic phase with the space group $P2_1/n$. Interestingly, in the extended structure of **3**, molecules of $[Cu_4L_4''(DMF)_4]$ interdigitate in an identical manner to that of **2**. The bulkier carbazole moiety pushes the cages further apart within the 2D layers to give an average inter-cage Cu···Cu distance of 21.1 Å (Fig. 6e).

We confirmed the bulk purity of **2** and **3** by IR spectroscopy and PXRD (Fig. S9b and S18†). The former revealed new C=N stretches at 1619 cm^{-1} and 1630 cm^{-1} for **2** and **3** respectively, as well as the absence of the aldehyde stretch (1698 cm^{-1}). Attempting other crystallisation conditions to obtain solvatomorphs of **2** and **3** led to the same crystal packing or the isolation of poorly crystalline precipitates that were not further investigated. By providing more opportunities for π–π

interactions, it is evident that the range of solvatomorphs may be limited compared to **1**. However, this may be advantageous for the crystal engineering of MOP solids; other functionalities (*e.g.* H-bonding) could be introduced through covalent PAM to control the structural rigidity, thus limiting the effect that coordinating solvent plays in determining the crystal packing.

Conclusions

In summary, we have demonstrated the remarkable propensity of an aldehyde-functionalised metal–organic polyhedron to form a range of unique crystal packings. In our system, five different solvatomorphs were isolated, which allowed us to compare their solvent exchange behaviour, phase transformations and porosity. Notably, one phase (**1e**) could only be obtained through the conversion of **1c** or **1d** in acetone, suggesting that certain solvatomorphs can act as templates for the formation of otherwise inaccessible crystal packings. A comparison of the N$_2$ adsorption profiles of pseudo-polymorphs of **1** revealed that different adsorbing forms are produced under analogous activation conditions. We also showed that the porosity of a non-porous phase can be switched on by solvent treatment. This demonstrates that the rich crystal-phase behaviour commonly observed for purely organic cages is also inherent to paddlewheel-based MOPs. Given their interest as functional materials, exploiting their solvatomorphism, structural flexibility and phase-dependant porosity may have implications for modulating their gas separation and catalytic properties.

Finally, we demonstrated that **1** can be covalently modified in solution *via* imine condensation. In the solid-state, the covalent extensions of **1** led to an interdigitated 2D sheet-like motif, which was observed in both of the modified samples. We think that this approach may open up new avenues for the design and crystal engineering of porous MOP materials. Indeed, the assembly of hierarchical materials is an emerging field of research,[46–48] and the exterior modifications of **1** show promise for assembling COF-like materials from MOP building blocks. Efforts towards this goal are currently underway in our laboratory.

Conflicts of interest

There are no conflicts to declare.

Acknowledgements

National Computing Infrastructure (NCI), CSIRO Pearcey cluster, and Pawsey supercomputing facilities.

Notes and references

‡ Owing to the paramagnetic Cu$_2$ paddlewheel node of **1–3**, proton resonances in close proximity to the metal node are significantly broadened.[26]

§ During the transformation of **1c/d** to **1b**, the crystals of the parent phase fragment rapidly. Despite the insolubility of **1** in MeOH and even mixtures of DMF/MeOH, we cannot completely rule out the possibility of an extremely rapid recrystallisation.

1 T. Hasell and A. I. Cooper, *Nat. Rev. Mater.*, 2016, **1**, 16053.

2 D. J. Tranchemontagne, Z. Ni, M. O'Keeffe and O. M. Yaghi, *Angew. Chem., Int. Ed.*, 2008, **47**, 5136–5147.

3 F. Beuerle and B. Gole, *Angew. Chem., Int. Ed.*, 2018, **57**, 4850–4878.

4 H. Furukawa, K. E. Cordova, M. O'Keeffe and O. M. Yaghi, *Science*, 2013, **341**, 1230444.

5 X. Feng, X. Ding and D. Jiang, *Chem. Soc. Rev.*, 2012, **41**, 6010–6022.

6 J. T. A. Jones, T. Hasell, X. Wu, J. Bacsa, K. E. Jelfs, M. Schmidtmann, S. Y. Chong, D. J. Adams, A. Trewin, F. Schiffman, F. Cora, B. Slater, A. Steiner, G. M. Day and A. I. Cooper, *Nature*, 2011, **474**, 367–371.

7 Z. Wang, N. Sikdar, S.-Q. Wang, X. Li, M. Yu, X.-H. Bu, Z. Chang, X. Zou, Y. Chen, P. Cheng, K. Yu, M. J. Zaworotko and Z. Zhang, *J. Am. Chem. Soc.*, 2019, **141**, 9408–9414.

8 J. T. A. Jones, D. Holden, T. Mitra, T. Hasell, D. J. Adams, K. E. Jelfs, A. Trewin, D. J. Willock, G. M. Day, J. Bacsa, A. Steiner and A. I. Cooper, *Angew. Chem., Int. Ed.*, 2011, **50**, 749–753.

9 A. Avellaneda, P. Valente, A. Burgun, J. D. Evans, A. W. Markwell-Heys, D. Rankine, D. J. Nielsen, M. R. Hill, C. J. Sumby and C. J. Doonan, *Angew. Chem., Int. Ed.*, 2013, **52**, 3746–3749.

10 S. Bera, K. Dey, T. K. Pal, A. Halder, S. Tothadi, S. Karak, M. Addicoat and R. Banerjee, *Angew. Chem., Int. Ed.*, 2019, **58**, 4243–4247.

11 A. C. Sudik, A. R. Millward, N. W. Ockwig, A. P. Côté, J. Kim and O. M. Yaghi, *J. Am. Chem. Soc.*, 2005, **127**, 7110–7118.

12 J. Park, Z. Perry, Y. P. Chen, J. Bae and H. C. Zhou, *ACS Appl. Mater. Interfaces*, 2017, **9**, 28064–28068.

13 W.-H. Xing, H.-Y. Li, X.-Y. Dong and S.-Q. Zang, *J. Mater. Chem. A*, 2018, **6**, 7724–7730.

14 L. Chen, T. Yang, H. Cui, T. Cai, L. Zhang and C.-Y. Su, *J. Mater. Chem. A*, 2015, **3**, 20201–20209.

15 S. Furukawa, N. Horike, M. Kondo, Y. Hijikata, A. Carné-Sánchez, P. Larpent, N. Louvain, S. Diring, H. Sato, R. Matsuda, R. Kawano and S. Kitagawa, *Inorg. Chem.*, 2016, **55**, 10843–10846.

16 G. R. Lorzing, B. A. Trump, C. M. Brown and E. D. Bloch, *Chem. Mater.*, 2017, **29**, 8583–8587.

17 W. Lu, D. Yuan, A. Yakovenko and H.-C. Zhou, *Chem. Commun.*, 2011, **47**, 4968–4970.

18 H. Vardhan, M. Yusubov and F. Verpoort, *Coord. Chem. Rev.*, 2016, **306**, 171–194.

19 M. Jaya Prakash, M. Oh, X. Liu, K. N. Han, G. H. Seong and M. S. Lah, *Chem. Commun.*, 2010, **46**, 2049–2051.

20 Y. H. Kang, X. D. Liu, N. Yan, Y. Jiang, X. Q. Liu, L. B. Sun and J. R. Li, *J. Am. Chem. Soc.*, 2016, **138**, 6099–6102.

21 Y.-H. Kang, N. Yan, Z.-Y. Gao, P. Tan, Y. Jiang, X.-Q. Liu and L.-B. Sun, *J. Mater. Chem. A*, 2017, **5**, 5278–5282.

22 O. Barreda, G. Bannwart, G. P. A. Yap and E. D. Bloch, *ACS Appl. Mater. Interfaces*, 2018, **10**, 11420–11424.

23 T.-F. Liu, Y.-P. Chen, A. A. Yakovenko and H.-C. Zhou, *J. Am. Chem. Soc.*, 2012, **134**, 17358–17361.

24 Z. Niu, S. Fang, X. Liu, J.-G. Ma, S. Ma and P. Cheng, *J. Am. Chem. Soc.*, 2015, **137**, 14873–14876.

25 D. A. Roberts, B. S. Pilgrim and J. R. Nitschke, *Chem. Soc. Rev.*, 2018, **47**, 626–644.

26 V. Brega, M. Zeller, Y. He, H. Peter Lu and J. K. Klosterman, *Chem. Commun.*, 2015, **51**, 5077–5080.

27 A. Carné-Sánchez, J. Albalad, T. Grancha, I. Imaz, J. Juanhuix, P. Larpent, S. Furukawa and D. Maspoch, *J. Am. Chem. Soc.*, 2019, **141**, 4094–4102.

28 R. W. Larsen, *J. Am. Chem. Soc.*, 2008, **130**, 11246–11247.

29 M. Kato, H. B. Jonassen and J. C. Fanning, *Chem. Rev.*, 1964, **64**, 99–128.

30 W. M. Bloch, R. Babarao, M. R. Hill, C. J. Doonan and C. J. Sumby, *J. Am. Chem. Soc.*, 2013, **135**, 10441–10448.

31 A. Schneemann, V. Bon, I. Schwedler, I. Senkovska, S. Kaskel and R. A. Fischer, *Chem. Soc. Rev.*, 2014, **43**, 6062–6096.

32 G. A. Craig, P. Larpent, S. Kusaka, R. Matsuda, S. Kitagawa and S. Furukawa, *Chem. Sci.*, 2018, **9**, 6463–6469.

33 J. M. Teo, C. J. Coghlan, J. D. Evans, E. Tsivion, M. Head-Gordon, C. J. Sumby and C. J. Doonan, *Chem. Commun.*, 2016, **52**, 276–279.

34 W. M. Bloch and C. J. Sumby, *Chem. Commun.*, 2012, **48**, 2534–2536.

35 T. M. Muzioł, N. Tereba, R. Podgajny, D. Kędziera and G. Wrzeszcz, *Dalton Trans.*, 2019, **48**, 11536–11546.

36 G. Kresse and J. Hafner, *Phys. Rev. B: Condens. Matter Mater. Phys.*, 1993, **48**, 13115–13118.

37 S. L. Price, *Acc. Chem. Res.*, 2009, **42**, 117–126.

38 E. O. Pyzer-Knapp, H. P. G. Thompson, F. Schiffmann, K. E. Jelfs, S. Y. Chong, M. A. Little, A. I. Cooper and G. M. Day, *Chem. Sci.*, 2014, **5**, 2235–2245.

39 S. Grimme, S. Ehrlich and L. Goerigk, *J. Comput. Chem.*, 2011, **32**, 1456–1465.

40 J. P. Perdew, K. Burke and M. Ernzerhof, *Phys. Rev. Lett.*, 1996, **77**, 3865–3868.

41 G. Kresse and D. Joubert, *Phys. Rev. B: Condens. Matter Mater. Phys.*, 1999, **59**, 1758–1775.

42 S. Mollick, S. Mukherjee, D. Kim, Z. Qiao, A. V. Desai, R. Saha, Y. D. More, J. Jiang, M. S. Lah and S. K. Ghosh, *Angew. Chem., Int. Ed.*, 2019, **58**, 1041–1045.

43 Y. Gong, Y. Zhang, C. Qin, C. Sun, X. Wang and Z. Su, *Angew. Chem., Int. Ed.*, 2019, **58**, 780–784.

44 S. Mollick, S. Fajal, S. Mukherjee and S. K. Ghosh, *Chem.–Asian J.*, 2019, **14**, 3096–3108.

45 M. Matsumoto, R. R. Dasari, W. Ji, C. H. Feriante, T. C. Parker, S. R. Marder and W. R. Dichtel, *J. Am. Chem. Soc.*, 2017, **139**, 4999–5002.

46 S. Datta, M. L. Saha and P. J. Stang, *Acc. Chem. Res.*, 2018, **51**, 2047–2063.

47 G. Lal, M. Derakhshandeh, F. Akhtar, D. M. Spasyuk, J.-B. Lin, M. Trifkovic and G. K. H. Shimizu, *J. Am. Chem. Soc.*, 2019, **141**, 1045–1053.

48 A. Carné-Sánchez, G. A. Craig, P. Larpent, T. Hirose, M. Higuchi, S. Kitagawa, K. Matsuda, K. Urayama and S. Furukawa, *Nat. Commun.*, 2018, **9**, 2506.

49 N. P. Cowieson, D. Aragao, M. Clift, D. J. Ericsson, C. Gee, S. J. Harrop, N. Mudie, S. Panjikar, J. R. Price, A. Riboldi-Tunnicliffe, R. Williamson and T. Caradoc-Davies, *J. Synchrotron Radiat.*, 2015, **22**, 187–190.